The effective Reynolds exponent of turbulent pipe heat transfer and the rigidity of the Dittus–Boelter correlation

Ivan Otić*[1] and Özgür Ertunç[2]

[1]Institute for Thermal Energy Technology and Safety, Karlsruhe Institute of Technology, Eggenstein-Leopoldshafen, Germany

[2]Fluid Dynamics and Spray Laboratory, Mechanical Engineering, Özyeğin University, İstanbul, Türkiye

Abstract

The Lyon integral for fully developed turbulent pipe flow of a constant-property fluid is evaluated with a closure containing no constant fitted to heat-transfer data: the Musker eddy viscosity constrained by the velocity log law, the Reichardt outer factor, and the Kays–Crawford turbulent Prandtl number. The bulk temperature takes the three-term form $\theta_b^+ = (\mathrm{Pr}_{t\infty}/\kappa)\ln \mathrm{Re}_\tau + \beta(\mathrm{Pr}) + C_0$, so that $\mathrm{Nu} = 2\,\mathrm{Re}_\tau\,\mathrm{Pr}/\theta_b^+$, with the thermal log-law intercept $\beta(\mathrm{Pr})$ and the core constant C_0 returned by the quadrature. The intercept agrees to within 4 % with the recent DNS-based expression of Pirozzoli over $0.5 \le \mathrm{Pr} \le 16$ and independently supports the small coefficient of $\ln \mathrm{Pr}$ against the classical Kader–Yaglom value. The Nusselt number lies within ± 3.6 % of isoflux pipe simulations at $\mathrm{Pr} = 0.71$ and within -7 to $+2$ % of isothermal-wall DNS across the Prandtl range. The Reynolds dependence is a power law modulated by two logarithms, that of the momentum log layer in the friction factor and that of the thermal log layer in the resistance, and the effective exponent $n_{\mathrm{eff}} = \partial \ln \mathrm{Nu}/\partial \ln \mathrm{Re}$ increases from 0.72 to 0.89 over $10^4 \le \mathrm{Re} \le 10^6$ and $0.7 \le \mathrm{Pr} \le 14$, between the asymptotes $1-2/\ln \mathrm{Re}$ and $1-1/\ln \mathrm{Re}$; exponents from $\mathrm{Pr} = 1$ DNS follow the predicted increase to within 0.03. A power law fitted to this surface has one degree of freedom: prefactor and exponent are related by $\mathrm{d}\ln C/\mathrm{d}n = -\ln \mathrm{Re}_0$ at the calibration Reynolds number Re_0. The Dittus–Boelter pair $(C, n) = (0.023, 0.8)$ of $\mathrm{Nu} = C\,\mathrm{Re}^n\mathrm{Pr}^m$ is the tangent to the surface at the classical calibration conditions, and the coefficient pairs of two later correlations of the same form, calibrated on supercritical-water experiments by Bishop and by Swenson, lie on the predicted locus at separations that recover their calibration Reynolds numbers, $\mathrm{Re}_0 \approx 1.7 \times 10^5$ and 4.9×10^5. The prefactor is the structural compensation for the exponent: a power-law correlation cannot follow a flow whose bulk Reynolds number varies along the pipe, nor be made to by adjusting the exponent.

1 Introduction

Turbulent heat transfer in a smooth pipe is described by two families of correlation that have coexisted for ninety years. The first is logarithmic. It follows from the overlap-layer structure of the mean velocity and temperature profiles and expresses the Nusselt number through additive resistances, each carrying a logarithm of the Reynolds number [6, 10, 19, 20]. The second is the power law $\mathrm{Nu} = C\,\mathrm{Re}^n\,\mathrm{Pr}^m$, of which the Dittus–Boelter form [3] with $(C, n) = (0.023, 0.8)$ remains the baseline of engineering practice: it is the default closure of the one-dimensional system codes used in thermal-hydraulic design, see e.g. [15, 27], and the majority of the more than two hundred property-corrected correlations proposed for fluids at supercritical pressure are multiplicative extensions of

*Corresponding author: `ivan.otic@kit.edu`

its $\mathrm{Re}^n\,\mathrm{Pr}^m$ base, see e.g. [8, 21, 32]. The two forms are not mutually consistent. A logarithmic expression has no constant Reynolds exponent. A power law does. The usual interpretation of this discrepancy is practical: the power law is an approximation, adequate over the range across which it was calibrated and inaccurate outside it. The interpretation is correct but incomplete, because it treats C and n as independent parameters that happen to have been fitted together. The rigidity it implies is inconsistent with the established description of turbulent thermal convection, in which the leading-order exponent is an effective, range-dependent quantity and the prefactor a physically determined one [1, 7, 12, 28]. C and n are not independent, and the constraint that relates them is the subject of this paper.

Our approach is based on the Lyon integral [13], which is exact for fully developed constant-property pipe flow. Its solution requires an eddy viscosity and a turbulent Prandtl number. We apply the eddy viscosity of Musker [16], whose single constant is determined by the momentum log law, attenuated in the core by the outer factor of Reichardt [26], and the turbulent Prandtl number of Kays and Crawford [11].

The thermal log-law intercept $\beta(\mathrm{Pr})$ returned by this closure is the quantity introduced by Kader and Yaglom [10] and recently obtained in explicit algebraic form by Pirozzoli [23], who inferred the eddy viscosity of Musker [16] and a constant of an algebraic eddy-diffusivity profile from direct numerical simulation (DNS) at $\mathrm{Re}_\tau = 1137.6$ over $0.00625 \leq \mathrm{Pr} \leq 16$ [22] and integrated it under the inner-layer approximation. The present formulation requires no additional information from simulations or experiments, and the two determinations of $\beta(\mathrm{Pr})$ agree to within 4 % over more than a decade in Prandtl number. They also agree on the coefficient of $\ln \mathrm{Pr}$, on which the classical Kader–Yaglom expression differs (Section 2.1).

The solution of the Lyon integral yields a Nusselt number that is compared with results from three simulation databases, all of which treat the temperature as a passive scalar: the isothermal-wall pipe DNS of Pirozzoli [23] at $\mathrm{Re}_\tau = 1137.6$ across the Prandtl range $0.00625 \leq \mathrm{Pr} \leq 16$, the $\mathrm{Pr} = 1$ pipe DNS of Pirozzoli et al. [25] spanning $\mathrm{Re}_\tau = 180$–6000, and the pipe simulations of Straub et al. [29] at $\mathrm{Pr} = 0.71$ over $\mathrm{Re} = 5\,300$–$37\,700$ with isoflux, isothermal and mixed-type thermal boundary conditions. It is further compared with the correlations of Petukhov and Kirillov [19, 20] and of Gnielinski [6], the two established engineering forms that retain the logarithmic friction structure.

Three results follow. Section 4 introduces the effective Reynolds exponent, $n_{\text{eff}} = \partial \ln \mathrm{Nu}/\partial \ln \mathrm{Re}$ at fixed Prandtl number: the local slope of the exact scaling, and hence the exponent that any power law fitted over a narrow Reynolds window must adopt. Because the exact scaling carries two logarithms, n_{eff} is not constant. It is obtained in closed form as the product of a momentum deficit and a thermal deficit, and drifts across the engineering range between the asymptote $1 - 2/\ln \mathrm{Re}$, reached when the momentum and thermal log layers contribute equally, and $1 - 1/\ln \mathrm{Re}$, reached when the conductive sublayer dominates; the separation of the two measures the thermal share of the total resistance. The $\mathrm{Pr} = 1$ simulations of Pirozzoli et al. [25] confirm the drift and its magnitude over one and a half decades of Reynolds number. In Section 5 a power law fitted locally to this surface is shown to have a prefactor and an exponent tied by a single differential relation, so that the classical calibration pairs are coordinates of a tangency rather than independent choices; the Dittus–Boelter, Bishop and Swenson pairs lie on the predicted locus. Section 6 states the consequence for flows in which the bulk Reynolds number varies along the pipe. The clearest instance is heat transfer at supercritical pressure, where the viscosity decrease across the pseudocritical region changes Re severalfold along a single heated tube. The present paper is confined to the constant-property problem, on which every correlation of the Dittus–Boelter family rests. The two-part study [17, 18] carries the present result into the supercritical regime and tests it there against the experimental database.

2 The Lyon integral

Consider fully developed turbulent flow of a constant-property fluid in a smooth circular pipe of radius R, heated at a uniform wall heat flux q_w, under axisymmetric and thermally fully developed conditions. Let $r^* = r/R$, let $y = R - r$ be the wall distance, and wall units built on the friction velocity $u_\tau = \sqrt{\tau_w/\rho}$ and the friction temperature $T_\tau = q_w/(\rho\, c_p\, u_\tau)$: $y^+ = y\, u_\tau/\nu$, $u^+ = u/u_\tau$, $\theta^+ = (T_w - T)/T_\tau$. The friction Reynolds number is $\mathrm{Re}_\tau = u_\tau R/\nu$ and the bulk Reynolds number $\mathrm{Re} = u_b\, d/\nu = 2\, u_b^+\, \mathrm{Re}_\tau$, with u_b the bulk velocity and $d = 2R$ the pipe diameter. Because the axial temperature gradient is uniform across the section, the energy equation integrates once in the radial direction and the local radial heat flux is set by the enthalpy convected inside radius r,

$$\Phi(r^*) \equiv \frac{q(r)}{q_w} = \frac{2}{r^*} \int_0^{r^*} \frac{u}{u_b}\, r'\, \mathrm{d}r', \qquad \Phi(1) = 1. \tag{1}$$

With the eddy diffusivity for momentum ε_m and the turbulent Prandtl number Pr_t, the flux–gradient relation for the mean temperature reads

$$\frac{\mathrm{d}\theta^+}{\mathrm{d}y^+} = \frac{\Phi}{\mathrm{Pr}^{-1} + \varepsilon_m^+/\mathrm{Pr}_t}, \qquad \varepsilon_m^+ = \varepsilon_m/\nu. \tag{2}$$

The bulk temperature T_b is the velocity-weighted average of T over the cross-section, and the Nusselt number is defined on the wall-to-bulk temperature difference:

$$\theta_b^+ = 2 \int_0^1 \frac{u}{u_b}\, \theta^+\, r^*\, \mathrm{d}r^*, \qquad \mathrm{Nu} = \frac{\alpha\, d}{\lambda} = \frac{q_w\, d}{\lambda\,(T_w - T_b)} = \frac{2\,\mathrm{Re}_\tau\, \mathrm{Pr}}{\theta_b^+}. \tag{3}$$

Equations (1)–(3) are the Lyon integral [13]. Eliminating θ^+ between (2) and (3) by one integration by parts gives Lyon's single expression, in which θ_b^+ is the radial integral of $\mathrm{Re}_\tau\, \Phi^2 r^{*2}/(\mathrm{Pr}^{-1} + \varepsilon_m^+/\mathrm{Pr}_t)$. The two-step form is retained here because each step has a separate physical reading. The entire radius enters: the velocity profile through Φ and through the weight u/u_b in (3), and the core region through both. A wall-layer treatment replaces Φ by $1 - y^+/\mathrm{Re}_\tau$ and then by unity, and must supply the core contribution to θ_b^+ as an external constant. Retaining Φ requires a quadrature and returns that contribution as an output.

The closure requires $\varepsilon_m^+(y^+)$ and Pr_t. It is constructed so that no constant is fitted to pipe heat-transfer data or to any thermal simulation of this configuration: the eddy-viscosity constants belong to the momentum problem, and the turbulent Prandtl number is taken as an independently established transport ratio, cross-checked below against the momentum-to-thermal log-law slope ratio of the pipe DNS.

For the smooth pipe we take $u^+ = \kappa^{-1} \ln y^+ + B$ with $\kappa = 0.387$ and $B = 4.3$ [14, 24] and apply the algebraic eddy viscosity formulation of Musker [16],

$$\varepsilon_i^+ = \frac{\kappa\, {y^+}^3}{{y^+}^2 + \kappa/C}, \tag{4}$$

with the limits $\varepsilon_i^+ \to C\, {y^+}^3$ at the wall, as required by the continuity of the fluctuating velocity at a solid boundary, and $\varepsilon_i^+ \to \kappa\, y^+$ in the overlap layer. Following Musker, C is not free: it is determined by the requirement that the integrated constant-stress profile $u^+ = \int_0^{y^+} \mathrm{d}y'^+/(1 + \varepsilon_i^+)$ reproduce the log law (κ, B) above. This gives $C = 1.19 \times 10^{-3}$ (Musker's own value, obtained for $\kappa = 0.41$, is 1.09×10^{-3}; the difference is the sensitivity of the constraint to the log-law constants).

A single algebraic diffusivity is used across the whole radius, as is usual in eddy-viscosity modelling, but it is built in two steps kept apart by notation: ε_i^+ denotes the inner (wall-layer) form (4), which grows without bound as κy^+, whereas across the core the momentum eddy diffusivity does not continue to grow linearly but levels off. The full-radius diffusivity ε_m^+ entering (2) therefore follows from ε_i^+ by an outer attenuation. We take the outer factor of Reichardt [26],

$$\varepsilon_m^+ = \varepsilon_i^+ \, \frac{(1+r^*)\,(1+2\,r^{*2})}{6}, \qquad r^* = 1 - \frac{y^+}{\mathrm{Re}_\tau}, \tag{5}$$

which is unity at the wall and gives $\varepsilon_m^+ \to \kappa\,\mathrm{Re}_\tau/6$ on the axis. It contains no constant.

The closure is validated immediately against the pipe DNS of Pirozzoli et al. [25]. The full-radius integration of the momentum balance, $\mathrm{d}u^+/\mathrm{d}y^+ = (1 - y^+/\mathrm{Re}_\tau)/(1+\varepsilon_m^+)$, then returns $u_b^+ = 19.13$ at $\mathrm{Re}_\tau = 1137.6$ against the simulated 19.34 [25], and 23.55 at $\mathrm{Re}_\tau = 6019$ against 23.67. The bulk Reynolds number is thus obtained from the same profile that enters (1) and (3), and no external friction law is needed. Without the outer factor the same integration returns $u_b^+ = 17.6$ at $\mathrm{Re}_\tau = 1137.6$, a centreline deficit of order $1/\kappa$ that would propagate into Φ, into the weight u/u_b, and into the core resistance.

To complete the closure we use the turbulent Prandtl number correlation of Kays and Crawford [11],

$$\frac{1}{\mathrm{Pr}_t} = \frac{1}{2\,\mathrm{Pr}_{t\infty}} + \frac{c\,\mathrm{Pe}_t}{\sqrt{\mathrm{Pr}_{t\infty}}} - (c\,\mathrm{Pe}_t)^2 \left[1 - \exp\!\left(-\frac{1}{c\,\mathrm{Pe}_t\sqrt{\mathrm{Pr}_{t\infty}}}\right)\right], \qquad \mathrm{Pe}_t = \mathrm{Pr}\,\varepsilon_m^+, \tag{6}$$

with $\mathrm{Pr}_{t\infty} = 0.85$ and $c = 0.3$, which gives $\mathrm{Pr}_t \to 1.7$ at the wall, 0.96 at $y^+ = 20$ for $\mathrm{Pr} = 1$, and 0.85 wherever $\mathrm{Pe}_t \gg 1$. The overlap-layer value 0.85 is consistent with the ratio $\kappa/k_\theta = 0.387/0.459 = 0.84$ of the momentum and thermal log-law slopes measured in the pipe DNS [25]. The eddy diffusivity for heat follows as $\varepsilon_h^+ = \varepsilon_m^+/\mathrm{Pr}_t$.

Equations (1)–(6) are evaluated by quadrature on a logarithmically stretched wall-normal grid (see Data availability).

2.1 The thermal log-law intercept $\beta(\mathrm{Pr})$

In the constant-flux layer ($\Phi \to 1$), (2) integrates to a temperature profile whose large-y^+ behaviour is logarithmic. Writing

$$F(Y;\,\mathrm{Pr}) = \int_0^Y \frac{\mathrm{d}y^+}{\mathrm{Pr}^{-1} + \varepsilon_i^+/\mathrm{Pr}_t}, \qquad \beta(\mathrm{Pr}) \equiv \lim_{Y\to\infty}\Big[F(Y;\,\mathrm{Pr}) - \frac{\mathrm{Pr}_{t\infty}}{\kappa}\ln Y\Big], \tag{7}$$

both terms in the bracket diverge as $Y \to \infty$ and their difference converges: with $\varepsilon_i^+ \to \kappa y^+$ and $\mathrm{Pr}_t \to \mathrm{Pr}_{t\infty}$ the derivative of the bracket is $-(\mathrm{Pr}_{t\infty}^2/\mathrm{Pr})/[\kappa Y(\kappa Y + \mathrm{Pr}_{t\infty}/\mathrm{Pr})] = O(Y^{-2})$, which is integrable. The subtraction removes exactly the non-integrable part of the tail. The Prandtl-dependent physics of the conductive sublayer and buffer layer remains in the limit. Every decade of y^+ in the log layer contributes the same increment $(\mathrm{Pr}_{t\infty}/\kappa)\ln 10$ to the thermal resistance, so that the resistance of the inner layer separates exactly into a Prandtl-dependent, Reynolds-independent intercept and a universal logarithmic growth: $\theta^+ = (\mathrm{Pr}_{t\infty}/\kappa)\ln y^+ + \beta(\mathrm{Pr})$ for large y^+. Definition (7) is the thermal counterpart of the additive constant B of the velocity log law, $B = \lim_{Y\to\infty}[\,u^+(Y) - \kappa^{-1}\ln Y\,]$ with $u^+(Y) = \int_0^Y \mathrm{d}y^+/(1+\varepsilon_i^+)$. Setting $\mathrm{Pr} = 1$ and $\mathrm{Pr}_t \equiv 1$ makes the two integrands identical, so that

$$\beta(1)\big|_{\mathrm{Pr}_t\equiv 1} = B \tag{8}$$

identically. The quadrature returns 4.30. With the Kays–Crawford Pr_t, which departs from unity near the wall, the intercept at $\mathrm{Pr} = 1$ is instead $\beta(1) = 6.15$, not B.

Two limits characterise β. For sufficiently high Péclet number the resistance concentrates where $\varepsilon_i^+ \,\mathrm{Pr}/\mathrm{Pr}_t \sim 1$, inside the conductive sublayer, and the near-wall cubic behaviour of (4) gives

$$\beta(\mathrm{Pr}) \to \frac{2\pi}{3\sqrt{3}} \left(\frac{\mathrm{Pr}_{t,s}}{C}\right)^{1/3} \mathrm{Pr}^{2/3}, \tag{9}$$

the $\mathrm{Pr}^{2/3}$ law of the classical sublayer analyses, where $\mathrm{Pr}_{t,s}$ is the turbulent Prandtl number in the conductive sublayer. The quadrature gives $\beta/\mathrm{Pr}^{2/3} \to 11.6$ for $\mathrm{Pr} \to 10^3$, corresponding through (9) to $\mathrm{Pr}_{t,s} \approx 1.06$ in the Kays–Crawford model, and comparable to the constant 12.7 of the Petukhov–Kirillov formulation [19]. For $\mathrm{Pr} \sim 1$, β is of order B and the logarithmic term dominates the resistance.

Pr	0.5	0.7	1	2	4	7	16
present	1.22	3.37	6.15	13.57	24.98	38.67	70.60
Pirozzoli [23]	1.17	3.35	6.19	13.88	25.79	40.13	73.62
Kader [9]	1.61	3.73	6.50	14.08	26.09	40.91	76.46
deviation	+4.3 %	+0.7 %	−0.7 %	−2.2 %	−3.1 %	−3.6 %	−4.1 %

Table 1: Thermal log-law intercept $\beta(\mathrm{Pr})$ from Eq. (7), with ε_i^+ from (4) and Pr_t from (6), against the DNS-based expression $\beta = 12.2\,\mathrm{Pr}^{2/3} + 0.726 \ln \mathrm{Pr} - 6.03$ of Pirozzoli [23, Eq. 3.16] and the empirical profile of Kader [9], $\beta = (3.85\,\mathrm{Pr}^{1/3} - 1.3)^2 + 2.12 \ln \mathrm{Pr}$. Deviation: present relative to Pirozzoli.

Table 1 compares $\beta(\mathrm{Pr})$ evaluated from (7) with the explicit expression of Pirozzoli [23, Eq. 3.16], obtained by integrating an algebraic eddy-diffusivity profile of the same Musker structure whose single constant was fitted to the diffusivity inferred from DNS at $\mathrm{Re}_\tau = 1140$, and with the empirical profile of Kader [9]. Present and DNS-based values agree to within 4 % over $0.5 \le \mathrm{Pr} \le 16$, the present ones lying systematically below at $\mathrm{Pr} > 1$. The inputs are disjoint: here κ, B and C belong to the momentum problem and $\mathrm{Pr}_{t\infty}$ is a quantity established across many wall flows; there the profile constant was inferred from the thermal fields themselves. Agreement between two determinations with disjoint inputs supports both.

The two determinations also agree on a structural point on which the classical result differs. A least-squares fit of the present $\beta(\mathrm{Pr})$ to the functional form of Kader and Yaglom [10], $\beta = c_1 \mathrm{Pr}^{2/3} + c_2 \ln \mathrm{Pr} + c_3$, over $0.5 \le \mathrm{Pr} \le 16$ gives $(c_1,\, c_2,\, c_3) = (11.59,\, 0.89,\, -5.45)$ with a maximum residual of 0.02; Pirozzoli [23] obtains $(12.20,\, 0.726,\, -6.03)$ analytically and Kader and Yaglom [10] give $(12.5,\, 2.12,\, -5.3)$. The leading coefficient does not discriminate: by (9) it is set by the near-wall cubic coefficient of the eddy diffusivity alone, and the present $C = 1.19 \times 10^{-3}$ and the DNS-fitted $k_\theta^3/C_\theta^2 = 0.97 \times 10^{-3}$ of Pirozzoli [23] place it within a few per cent of one another. The coefficient of $\ln \mathrm{Pr}$ does discriminate. Pirozzoli [23] obtains $1/(3k_\theta) = 0.726$ where Kader and Yaglom [10] have $1/k_\theta = 2.12$, and identifies that difference as the source of the failure of the classical expression at low Prandtl number. The present construction, whose inputs contain no thermal simulation and no heat-transfer measurement, returns 0.89.

3 The Reynolds scaling of the Nusselt number

3.1 The three-term form

In the limit $y^+/\mathrm{Re}_\tau \to 0$, where $\Phi \to 1$, Eq. (2) integrates to $\theta^+ \to (\mathrm{Pr}_{t\infty}/\kappa)\ln y^+ + \beta(\mathrm{Pr})$, and because the log layer extends to a fixed fraction of the radius, the bulk temperature takes the three-term form

$$\theta_b^+ = \frac{\mathrm{Pr}_{t\infty}}{\kappa}\ln \mathrm{Re}_\tau + \beta(\mathrm{Pr}) + C_0, \qquad \mathrm{Nu} = \frac{2\,\mathrm{Re}_\tau\,\mathrm{Pr}}{\beta(\mathrm{Pr}) + (\mathrm{Pr}_{t\infty}/\kappa)\ln \mathrm{Re}_\tau + C_0}, \tag{10}$$

in which C_0 collects the contribution of the core: the departure of the temperature profile from the log law in the outer region and the velocity weighting in (3). The Reynolds number enters (10) twice – through the prefactor $\mathrm{Re}_\tau = \mathrm{Re}/(2u_b^+)$, governed by the momentum log layer through the friction law, and through $\ln \mathrm{Re}_\tau$ in the denominator, the resistance of the thermal log layer. This double entry is the structural content of the result.

The constant C_0 is an output of the quadrature, not an input. At $\mathrm{Pr} \le 1$ it drifts from -1.2 to -2.0 over $150 \le \mathrm{Re}_\tau \le 3\times10^4$; at higher Prandtl number, where the log layer is short and the sublayer resistance has not reached its asymptotic value, it starts closer to zero (-0.7 at $\mathrm{Pr} = 14$, $\mathrm{Re}_\tau = 400$) and converges to the same -2.0 by $\mathrm{Re}_\tau = 3\times10^4$. The residual drift is the part of the core contribution that the three-term form does not represent. A wall-layer treatment must supply this constant from outside, and the standard means of doing so is the Reynolds analogy: at $\mathrm{Pr} = 1$ with $\mathrm{Pr}_t \equiv 1$ the thermal problem (2) is the momentum problem with Φ in place of $1 - y^+/\mathrm{Re}_\tau$, so that $\theta_b^+ \approx u_b^+$ and $\mathrm{Nu} \approx (f/8)\,\mathrm{Re}\,\mathrm{Pr}$, which fixes C_0 through the friction law.

The full-radius quadrature quantifies the approximation: at $\mathrm{Pr} = \mathrm{Pr}_t = 1$ it returns $\theta_b^+/u_b^+ =$ 1.10, 1.07, 1.04 and 1.03 at $\mathrm{Re}_\tau = 500$, 1140, 6000 and 3×10^4, the departure of the pipe from the exact Reynolds analogy being produced by Φ and by the weight u/u_b and decreasing with Reynolds number. Retaining Φ makes this departure an output rather than an assumption.

3.2 Comparison with simulation

Pr	0.5	1	2	4	16
Nu (DNS)	81.7	119.9	168.0	233.3	421.2
Nu (present)	76.1	114.1	166.0	234.0	429.8
deviation	−6.9 %	−4.8 %	−1.2 %	+0.3 %	+2.1 %

Table 2: Nusselt number from the Lyon integral (1)–(3) with the closure of Section 2, against the isothermal-wall pipe DNS of Pirozzoli [23, Table 1] at $\mathrm{Re}_\tau = 1137.6$.

Table 2 compares the Nusselt number from the full quadrature with the isothermal-wall pipe DNS of Pirozzoli [23] at $\mathrm{Re}_\tau = 1137.6$ ($\mathrm{Re} = 44\,000$). At this Reynolds number the momentum closure returns $u_b^+ = 19.13$ against the simulated 19.34 and $\mathrm{Re} = 43\,500$. The Nusselt number lies within -7 to $+2$ % of the DNS across $0.5 \le \mathrm{Pr} \le 16$, below at low and above at high Prandtl number, with the crossing near $\mathrm{Pr} = 3$. The Prandtl trend of the residual reflects the core: at $\mathrm{Pr} \lesssim 1$ a substantial part of θ_b^+ accumulates outside the log layer, where the closure consists of the outer factor and $\mathrm{Pr}_{t\infty}$ alone, whereas at $\mathrm{Pr} \gg 1$ the resistance is confined to the sublayer and the residual is that of $\beta(\mathrm{Pr})$ in Table 1.

Table 3 makes the same comparison at $\mathrm{Pr} = 0.71$ against the pipe simulations of Straub et al. [29] (DNS at $\mathrm{Re} = 5\,300$, wall-resolved LES above), which realise the uniform-flux, thermally fully

Re_τ	Re (sim.)	Re (present)	$\mathrm{Nu}_{\mathrm{IF}}$	$\mathrm{Nu}_{\mathrm{MBC}}$	$\mathrm{Nu}_{\mathrm{IT}}$	Nu (present)	dev. IF	dev. MBC
181	5 300	4 950	18.38	18.29	17.57	18.95	+3.1 %	+3.6 %
361	11 700	11 460	34.74	34.55	33.57	34.29	−1.3 %	−0.7 %
550	19 000	18 800	50.47	50.20	48.95	49.47	−2.0 %	−1.4 %
999	37 700	37 500	85.27	85.35	83.45	83.57	−2.0 %	−2.1 %

Table 3: Nusselt number at $\mathrm{Pr} = 0.71$ from the Lyon integral at the friction Reynolds numbers of the pipe simulations of Straub et al. [29] (dataset [30]; Re_τ converted from their diameter-based value), against the simulated values for the isoflux (IF), mixed (MBC) and isothermal (IT) thermal boundary conditions. Re (present) is the bulk Reynolds number returned by the momentum closure at the same Re_τ; deviations refer to IF and MBC.

developed configuration assumed by the Lyon integral and report the Nusselt number for three thermal boundary conditions on the same velocity field: isoflux (IF), isothermal (IT), and the mixed-type condition (MBC), in which the mean profile is of isoflux type while the fluctuations satisfy an isothermal wall condition. Against the isoflux and mixed-type conditions the present quadrature lies within ±3.6 % over Re = 5 300–37 700, and within 2 % for Re ≥ 11 700. The isothermal Nusselt numbers are 2–4.5 % lower, which is the size of the boundary-condition effect at this Prandtl number. The bulk Reynolds number returned by the momentum closure at the simulated Re_τ is within 2 % of the simulated one for Re ≥ 11 700 and 6.5 % at Re = 5 300, where the log layer is barely established, see Eggels et al. [4].

Table 4 extends the comparison over Reynolds number at $\mathrm{Pr} = 1$, against the pipe DNS of Pirozzoli et al. [25] between $\mathrm{Re}_\tau = 180$ and 6019 (Re = 5 300–285 000).

Re_τ	Re (DNS)	u_b^+ (DNS)	u_b^+ (present)	Nu (DNS)	Nu (present)	dev.	n (DNS)	n_{eff} (present)
180.3	5 300	14.70	13.66	24.8	22.0	−11.3 %		
							0.761	0.742
495.3	17 000	17.16	16.80	60.2	54.1	−10.2 %		
							0.761	0.777
1136.6	44 000	19.36	19.12	124.2	114.0	−8.2 %		
							0.779	0.794
1976.0	82 500	20.88	20.61	202.7	187.7	−7.4 %		
							0.797	0.804
3028.1	133 000	21.96	21.74	296.5	276.2	−6.8 %		
							0.787	0.814
6019.4	285 000	23.67	23.55	540.0	515.5	−4.5 %		

Table 4: Reynolds sweep at $\mathrm{Pr} = 1$: Lyon integral at the friction Reynolds numbers of the pipe DNS of Pirozzoli et al. [25, Table 1], isothermal wall with constant-mean-temperature forcing. u_b^+ and Re (present) are returned by the momentum closure at the same Re_τ. The last column is the secant exponent $\Delta \ln \mathrm{Nu} / \Delta \ln \mathrm{Re}$ between consecutive DNS entries, placed at the geometric-mean Reynolds number, against the present n_{eff} of Eq. (14) at that Reynolds number.

The momentum closure follows the simulated bulk velocity to within 1–2 % for $\mathrm{Re}_\tau \geq 495$. The Nusselt number lies 4.5–11 % below the DNS, the deficit decreasing monotonically with Reynolds number. Two circumstances bear on this deficit. First, the thermal forcing of these simulations is an isothermal wall with a spatially uniform, time-dependent source term (constant-mean-temperature forcing), which Pirozzoli et al. [25] note "tends to slightly overpredict the heat flux" relative to the uniform-flux configuration. The isoflux–isothermal difference measured by Straub et al. [29] at $\mathrm{Pr} = 0.71$ is 2–4.5 % in the direction opposite to the present deficit, and the isothermal-wall Nusselt number of Pirozzoli [23] at the same $\mathrm{Re}_\tau = 1137.6$ is 3.5 % below the value in Table 4. Second, the same DNS lie 4–7 % above the Gnielinski correlation and 11–13 % above the Petukhov–Kirillov correlation over the whole sweep, whereas the isoflux simulations of Straub et al. [29] lie within 1–4 % of Gnielinski. The present quadrature is consistent with the latter two. The comparison of Table 4 is therefore used for the quantity to which a uniform offset of the level is relevant: the slope of $\ln \mathrm{Nu}$ against $\ln \mathrm{Re}$, which is the subject of Section 4.

3.3 Comparison with the logarithmic correlations

Equation (10) has the structure of the two established engineering formulations that retain the friction factor: the correlation of Petukhov and Kirillov [19, 20],

$$\mathrm{Nu}_{\mathrm{PK}} = \frac{(f/8)\,\mathrm{Re}\,\mathrm{Pr}}{1.07 + 12.7\,\sqrt{f/8}\,\left(\mathrm{Pr}^{2/3} - 1\right)}, \tag{11}$$

and that of Gnielinski [6],

$$\mathrm{Nu}_{\mathrm{G}} = \frac{(f/8)\,(\mathrm{Re} - 1000)\,\mathrm{Pr}}{1 + 12.7\,\sqrt{f/8}\,\left(\mathrm{Pr}^{2/3} - 1\right)}, \tag{12}$$

both evaluated as published with the Filonenko friction factor $f = (0.790 \ln \mathrm{Re} - 1.64)^{-2}$ [5]. Rewriting the denominator of (11) in the present normalisation,

$$\mathrm{Nu}_{\mathrm{PK}} = \frac{2\,\mathrm{Re}_\tau\,\mathrm{Pr}}{12.7\,(\mathrm{Pr}^{2/3} - 1) + 1.07\,u_b^+}, \tag{13}$$

exhibits the correspondence term by term: the first term of the denominator is the sublayer intercept (9), and the second, through the friction law $u_b^+ = \kappa^{-1} \ln \mathrm{Re}_\tau + \mathrm{const}$, is the $\ln \mathrm{Re}_\tau$ resistance of the thermal log layer with an effective slope $1.07/\kappa$ in place of $\mathrm{Pr}_{t\infty}/\kappa$. The present derivation obtains the same structure from the Lyon integral and the closure chain alone. Numerically (Table 5), the quadrature exceeds (11) by 0–9 % over $10^4 \le \mathrm{Re} \le 10^6$ and $0.7 \le \mathrm{Pr} \le 14$, the excess growing with Reynolds number at low Prandtl number, and lies within ±4 % of (12) for $\mathrm{Re} \ge 10^5$. The larger positive deviation from Gnielinski at $\mathrm{Re} = 10^4$ and high Prandtl number reflects the $(\mathrm{Re} - 1000)$ shift introduced in (12) for the transitional range.

	Pr				
Re	0.7	1	3	7	14
$\mathrm{Nu}/\mathrm{Nu}_{\mathrm{PK}}$					
10^4	1.010	1.002	1.011	1.032	1.050
10^5	1.067	1.053	1.038	1.042	1.050
10^6	1.093	1.078	1.054	1.050	1.052
$\mathrm{Nu}/\mathrm{Nu}_{\mathrm{G}}$					
10^4	1.035	1.041	1.083	1.121	1.150
10^5	0.997	0.994	1.006	1.025	1.042
10^6	1.015	1.009	1.008	1.020	1.032

Table 5: Ratio of the Nusselt number from the Lyon integral to the Petukhov–Kirillov correlation (11) and to the Gnielinski correlation (12), both evaluated with the Filonenko friction factor.

4 The effective Reynolds exponent

4.1 Closed form and asymptotes

The scaling (10) is not a power law. Over any finite Reynolds range it is locally approximated by $\mathrm{Re}^{n_{\mathrm{eff}}}$ with the effective exponent $n_{\mathrm{eff}} = \partial \ln \mathrm{Nu}/\partial \ln \mathrm{Re}$ at fixed Prandtl number. Logarithmic differentiation of (3) through $\mathrm{Re} = 2u_b^+ \mathrm{Re}_\tau$, with $\mathrm{d}u_b^+/\mathrm{d}\ln \mathrm{Re}_\tau = 1/\kappa$ from the friction law and $\mathrm{d}\theta_b^+/\mathrm{d}\ln \mathrm{Re}_\tau = \mathrm{Pr}_{t\infty}/\kappa$ from (10), gives

$$n_{\mathrm{eff}}(\mathrm{Re},\,\mathrm{Pr}) \equiv \left.\frac{\partial \ln \mathrm{Nu}}{\partial \ln \mathrm{Re}}\right|_{\mathrm{Pr}} = \underbrace{\frac{u_b^+}{u_b^+ + 1/\kappa}}_{\text{momentum}} \times \underbrace{\left(1 - \frac{\mathrm{Pr}_{t\infty}/\kappa}{\theta_b^+}\right)}_{\text{thermal}}. \tag{14}$$

Each factor is a deficit from unity produced by one of the two logarithms of the problem: the first is the contribution of the momentum log layer, contained in the friction law and independent of the Prandtl number; the second is that of the thermal log layer, Prandtl-dependent through $\beta(\mathrm{Pr})$ in θ_b^+. Evaluated with the log-law constants $1/\kappa$ and $\mathrm{Pr}_{t\infty}/\kappa$, (14) reproduces the exponent obtained by direct differentiation of the quadrature to within 0.008 over $10^4 \le \mathrm{Re} \le 10^6$; with the derivatives themselves taken from the quadrature the two agree to 10^{-4}. A power law holds n_{eff} constant by construction; (14) therefore quantifies the departure of any power law from the exact behaviour as a function of Re and Pr.

Writing $L = \ln \mathrm{Re}_\tau$, $u_b^+ \simeq L/\kappa$ and $\theta_b^+ \simeq (\mathrm{Pr}_{t\infty}/\kappa)(L + \kappa\beta/\mathrm{Pr}_{t\infty})$ to leading order,

$$n_{\mathrm{eff}} \simeq 1 - \frac{1}{L} - \frac{1}{L + \kappa\,\beta(\mathrm{Pr})/\mathrm{Pr}_{t\infty}} + O(L^{-2}), \tag{15}$$

with two limits. For Pr of order unity the thermal intercept is small against the thermal logarithm, the two deficits are equal, and

$$n_{\mathrm{eff}} \to 1 - \frac{2}{\ln \mathrm{Re}}, \tag{16}$$

the Reynolds-analogy result $\mathrm{Nu} \sim (f/8)\,\mathrm{Re}\,\mathrm{Pr} \sim \mathrm{Re}/(\ln \mathrm{Re})^2$, in which both logarithms belong to one and the same profile, once in the momentum problem and once in the thermal one. For $\beta(\mathrm{Pr}) \gg L\,\mathrm{Pr}_{t\infty}/\kappa$ the thermal resistance is dominated by the conductive sublayer, the second deficit vanishes, and

$$n_{\mathrm{eff}} \to 1 - \frac{1}{\ln \mathrm{Re}}, \tag{17}$$

the result of a sublayer-only analysis: the resistance lies below the thermal log layer, θ_b^+ becomes Reynolds-independent, and the entire Reynolds dependence enters through the prefactor Re_τ, i.e. through the momentum log layer alone. Since $\beta \sim \mathrm{Pr}^{2/3}$ grows algebraically while L grows logarithmically, (17) is approached from below as Pr increases at fixed Re, and (16) is recovered as $\mathrm{Pr} \to 1$. Equations (16) and (17) are leading-order asymptotes, not bounds. At finite Reynolds number the difference between $\ln \mathrm{Re}$ and $\ln \mathrm{Re}_\tau$ and the additive constants of the two log laws shift the exact exponent by a few hundredths in either direction.

4.2 The exponent surface

Table 6 and Fig. 1(a) give the exponent from the full quadrature. Over $10^4 \le \mathrm{Re} \le 10^6$ and $0.7 \le \mathrm{Pr} \le 14$ the effective exponent increases monotonically in both arguments from 0.72 to 0.89; its variation per decade of Reynolds number is 0.02–0.05 throughout. The value 0.8 is a contour of this surface: it passes through $(\mathrm{Pr},\,\mathrm{Re}) \approx (0.7,\,1.7\times10^5)$, $(1,\,8\times10^4)$ and $(3,\,1.3\times10^4)$, and

Re	Pr				
	0.7	1	3	7	14
10^4	0.723	0.745	0.792	0.814	0.825
5×10^4	0.775	0.791	0.828	0.847	0.858
10^5	0.790	0.803	0.837	0.856	0.867
5×10^5	0.817	0.827	0.855	0.872	0.883
10^6	0.827	0.836	0.862	0.878	0.888

Table 6: Effective Reynolds exponent $n_{\text{eff}}(\text{Re}, \text{Pr})$ from the full quadrature, Eq. (14).

lies below $\text{Re} = 10^4$ for $\text{Pr} \geq 7$. The Reynolds sweep of Pirozzoli et al. [25] tests the drift directly at $\text{Pr} = 1$. The secant exponents between consecutive simulations, listed in Table 4 and plotted in Fig. 1(a), increase from 0.76 at $\text{Re} \approx 10^4$ to 0.80 at $\text{Re} \approx 10^5$ and agree with the predicted curve to within 0.03; the predicted values at the same Reynolds numbers are 0.74, 0.78, 0.79, 0.80 and 0.81. The DNS confirms both the magnitude of the exponent – well below the sublayer asymptote (17), which gives 0.89–0.92 over this range, and close to the Reynolds-analogy asymptote (16) – and its increase by 0.04 over one and a half decades. The last secant, between $\text{Re} = 1.33 \times 10^5$ and 2.85×10^5, lies 0.01 below its predecessor where the prediction continues to increase; a change of one per cent in either of the two Nusselt numbers concerned displaces that secant by 0.013, so that the decrease is within the resolution of the comparison. Whether the drift saturates or continues at higher Reynolds numbers requires simulations beyond $\text{Re}_\tau = 6000$.

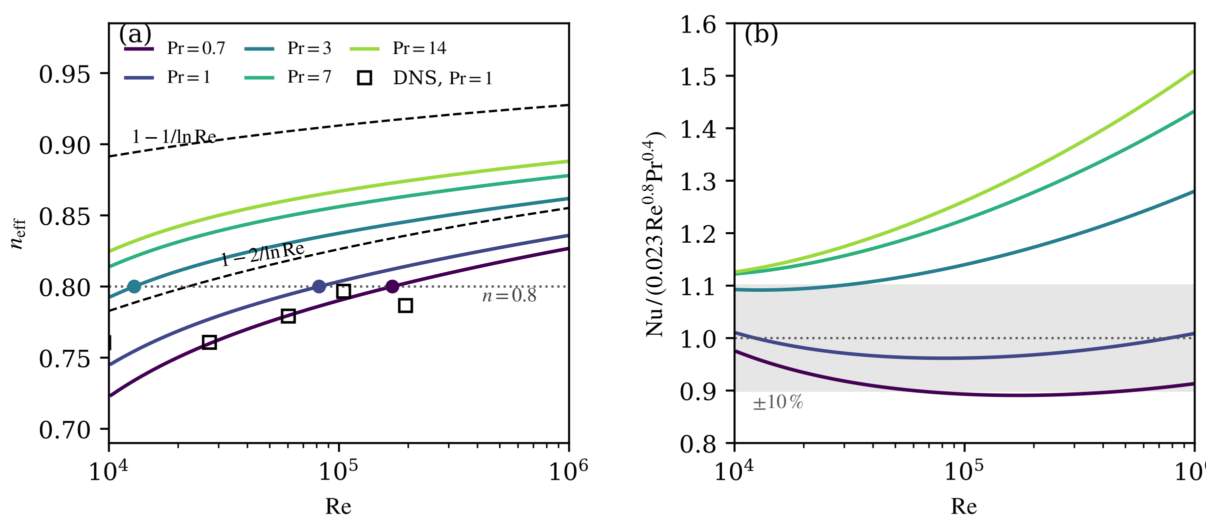

Figure 1: (a) Effective Reynolds exponent $n_{\text{eff}}(\text{Re}, \text{Pr})$ from the Lyon integral (solid), with the asymptotes (16) and (17) (dashed); circles mark the crossings of the $n = 0.8$ contour; open squares are the secant exponents of the $\text{Pr} = 1$ pipe DNS of Pirozzoli et al. [25], Table 4. (b) Ratio of the Nusselt number from the Lyon integral to the Dittus–Boelter correlation $0.023\,\text{Re}^{0.8}\text{Pr}^{0.4}$; the shaded band marks $\pm 10\,\%$. The rigid pair (0.023, 0.8) is tangent to the surface over the classical calibration window and detaches monotonically outside it.

The surface locates the classical power-law calibrations. The $n = 0.8$ contour passes through the conditions of the classical calibration databases and along that contour the Nusselt number of the Lyon integral is within about ten per cent of $0.023\,\mathrm{Re}^{0.8}\mathrm{Pr}^{0.4}$ (Fig. 1(b): ratios of 0.89, 0.96 and 1.09 at the three crossings). The Dittus–Boelter pair (0.023, 0.8) is therefore the tangent-plane approximation to the Lyon-integral surface at the conditions of its calibration: an accurate local approximation, and a structurally rigid one. Away from the tangency the pair detaches monotonically. By $\mathrm{Re} = 10^6$ the surface exceeds it by 43–51 % at $\mathrm{Pr} = 7$–14; at $\mathrm{Pr} \approx 0.7$ and $\mathrm{Re} \sim 2 \times 10^5$ it exceeds the surface by 12 %. These are the two directions in which the local (Re, Pr) of a supercritical-pressure flow moves along a heated pipe [17, 18].

The choice of friction law matters for this reading. The Blasius correlation $f = 0.316\,\mathrm{Re}^{-1/4}$ is a power-law approximation to the log-law friction factor, valid for $\mathrm{Re} \lesssim 10^5$ in isothermal, constant-property flow. Substituting it for the momentum factor of (14) would freeze that factor at 7/8; the thermal factor would still vary, so that even then the exponent is not constant, but the momentum half of the structure would be concealed. The full friction law is therefore retained throughout. That a turbulent transport law carries logarithmic factors, so that its effective exponent varies slowly rather than taking a constant value, is not peculiar to forced convection: Kraichnan [12], analysing turbulent free convection, obtained the analogous form $\mathrm{Nu} \sim \mathrm{Ra}^{1/2}(\ln \mathrm{Ra})^{-3/2}$; the mechanism and the power of the logarithm differ, but the structural point is the same.

5 Rigidity of the calibrated pair

5.1 The tangency constraint

Let a power law $\mathrm{Nu} = C\,\mathrm{Re}^n$ be fitted to the surface (3) over a calibration window centred on Re_0 at fixed Pr. Matching value and slope at the centroid, which differs from a least-squares fit in $\ln \mathrm{Nu}$ only at second order in the window width, gives

$$n = n_{\mathrm{eff}}(\mathrm{Re}_0,\, \mathrm{Pr}), \qquad \ln C = \ln \mathrm{Nu}(\mathrm{Re}_0,\, \mathrm{Pr}) - n \ln \mathrm{Re}_0. \tag{18}$$

The pair $(C,\, n)$ has one degree of freedom, not two: both coordinates are functions of the single tangency location Re_0. Differentiating the second of (18) along the surface and using the first to eliminate $\mathrm{d} \ln \mathrm{Nu} = n\, \mathrm{d} \ln \mathrm{Re}_0$ gives

$$\frac{\mathrm{d} \ln C}{\mathrm{d}n} = - \ln \mathrm{Re}_0, \tag{19}$$

which is the constraint. Prefactor and exponent trade against one another at a rate set by the logarithm of the calibration Reynolds number: a correlation with a larger exponent must carry a proportionately smaller prefactor, and the proportionality is set. Equation (19) contains no fitted quantity and no property of the fluid; it holds for any smooth Nu(Re) that is not itself a power law. The Lyon integral supplies the surface on which the tangency lies, and hence the value of n associated with a given Re_0 and Pr.

This is the analytical form of the entanglement of prefactor and exponent. The Dittus–Boelter prefactor 0.023 is not an independent empirical constant: it is the value that places $C\,\mathrm{Re}^{0.8}$ on the surface at the point where the local exponent equals 0.8, i.e. the structural compensation for the $\mathrm{Re}^{0.8}$ growth over the calibration window. Adjusting the exponent of a power-law correlation while retaining its prefactor, or comparing two correlations by their exponents alone, is therefore not admissible. Displacement along the locus (19) does not produce a different correlation but the same tangent expressed at a different calibration point. Similar structure is established in turbulent natural convection: there the leading-order exponent is an effective, range-dependent quantity rather than a universal constant [1, 7, 12], and the prefactor can be estimated from the flow structure rather than fitted to heat-transfer data [12]. Equation (19) is the forced-convection expression of that entanglement.

Equation (19) is testable without any data, using only published correlation coefficients. Taking Dittus–Boelter $(C, n) = (0.023, 0.8)$ as reference and reading the implied Re_0 from the finite difference $\ln \mathrm{Re}_0 = -\Delta \ln C/\Delta n$ gives Table 7.

correlation	C	n	implied Re_0
Dittus–Boelter [3]	0.023	0.8	reference
Bishop [2]	0.0069	0.90	1.7×10^5
Swenson [31]	0.00459	0.923	4.9×10^5

Table 7: Calibration Reynolds numbers implied by the locus (19), taking Dittus–Boelter as reference. Coefficients as tabulated in the sources cited.

Both implied values fall inside the Reynolds-number range of the supercritical-water experiments against which those correlations were calibrated [2, 18, 31]. This is the test of (19): three correlation pairs, obtained independently over three decades with different fluids and different apparatus, are displaced along the predicted locus rather than scattered about it, and the displacement recovers their calibration conditions. No property of the fluid enters the calculation. The Bishop and Swenson correlations carry, beyond the (C, n) pair, property-ratio factors and Prandtl exponents that differ from the Dittus–Boelter form; the locus (19) concerns only the Reynolds pair, which those multiplicative factors leave untouched, and the comparison is made at that level. Figure 2 places the three pairs in the $(n, \ln C)$ plane against the family of lines (19).

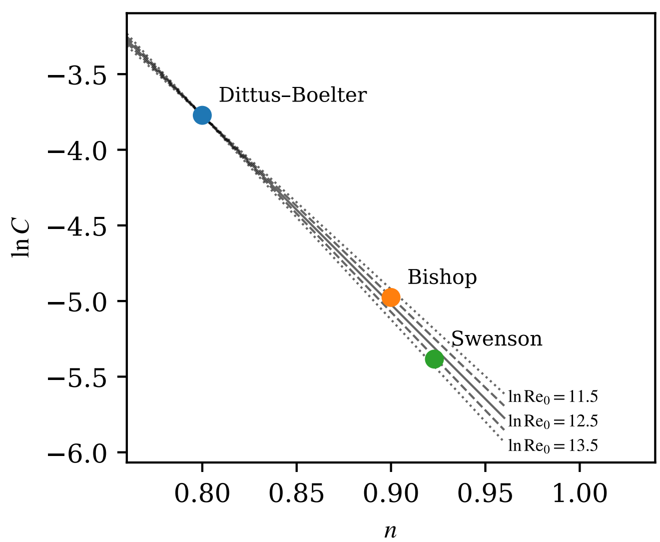

Figure 2: The classical correlation pairs in the $(n, \ln C)$ plane, against the family of tangency loci (19) at fixed $\ln \mathrm{Re}_0$ (grey). The three pairs are displaced along the locus rather than scattered off it; their separations recover the calibration Reynolds numbers of Table 7.

The rigidity has an operational consequence. Consider a heated pipe along which the bulk Reynolds number varies by a factor r between inlet and outlet, as it does whenever the viscosity or density of the fluid changes substantially along the pipe. A single power law is tangent to the true surface at one Re_0, and by (18) its logarithmic error at $\mathrm{Re} = r\,\mathrm{Re}_0$ is

$$\ln \frac{\mathrm{Nu}_{\text{power law}}}{\mathrm{Nu}} = -\int_{\mathrm{Re}_0}^{r\mathrm{Re}_0} \left[n_{\text{eff}}(\mathrm{Re}') - n\right] \mathrm{d}\ln \mathrm{Re}', \tag{20}$$

which is a monotone function of r because n_{eff} is monotone in Re. The detachment is one-sided: a correlation calibrated at the low-Reynolds end of its range over-predicts downstream, and one calibrated at the high end under-predicts upstream. It cannot be centred by adjusting n, because (19) displaces C with it and merely relocates the tangency. Only a departure from the power-law form removes it.

The magnitude of the constant-property detachment follows from Fig. 1(b). Because n_{eff} varies by only a few hundredths per decade, the error accumulated by a tangent pair over a factor of three in Reynolds number is small – 1.3 % for the Dittus–Boelter pair from its tangency at $\mathrm{Re} = 8 \times 10^4$, $\mathrm{Pr} = 1$ – and becomes significant only over decades: the same pair, tangent at $\mathrm{Re} = 1.3 \times 10^4$ for $\mathrm{Pr} = 3$, lies 4 % below the surface at 10^5 and 17 % at 10^6, and for $\mathrm{Pr} = 7$ the surface departs from it by 10 % per decade above 10^4. The scope of this result is limited to constant-property flow, and the detachment it predicts is present before any property variation is admitted. In flows with strong property gradients, and in supercritical-pressure fluids in particular, a second and generally larger source of correlation error is active – the property ratios that the multiplicative extensions of the Dittus–Boelter base are intended to absorb – and the two contributions are not separable by inspection. The present result establishes the base-line: the part of the departure that persists when properties are uniform, and that no reparametrisation of the exponent removes. Its interaction with the variable-property contribution is examined in Otić and Ertunç [17, 18], where the present result is used and tested against supercritical-pressure experiments.

6 Conclusions

The first result is a closed form. The Lyon integral for fully developed constant-property pipe flow, evaluated over the full radius with a closure containing no constant fitted to heat-transfer data, gives $\mathrm{Nu} = 2\,\mathrm{Re}_\tau\,\mathrm{Pr}/[\beta(\mathrm{Pr}) + (\mathrm{Pr}_{t\infty}/\kappa)\ln \mathrm{Re}_\tau + C_0]$, with the thermal log-law intercept $\beta(\mathrm{Pr})$ and the core constant C_0 both returned by the quadrature. The intercept agrees to within 4 % with the DNS-based expression of Pirozzoli [23] over $0.5 \le \mathrm{Pr} \le 16$ and, from disjoint inputs, confirms the coefficient 0.7–0.9 of $\ln \mathrm{Pr}$ against the Kader–Yaglom value 2.12. The Nusselt number lies within ± 3.6 % of the isoflux pipe simulations of Straub et al. [29] at $\mathrm{Pr} = 0.71$, within -7 to $+2$ % of the isothermal-wall DNS of Pirozzoli [23] across the Prandtl range, and within ± 4 % of the Gnielinski correlation for $\mathrm{Re} \ge 10^5$.

The second result is structural. The Reynolds dependence of the Nusselt number is a power law modulated by two logarithms, that of the momentum log layer in the friction factor and that of the thermal log layer in the resistance. The effective exponent factorises accordingly, $n_{\text{eff}} = [u_b^+/(u_b^+ + 1/\kappa)]\,[1 - (\mathrm{Pr}_{t\infty}/\kappa)/\theta_b^+]$, and increases from 0.72 to 0.89 over $10^4 \le \mathrm{Re} \le 10^6$ and $0.7 \le \mathrm{Pr} \le 14$, between the asymptotes $1 - 2/\ln \mathrm{Re}$ and $1 - 1/\ln \mathrm{Re}$; the $\mathrm{Pr} = 1$ Reynolds sweep of Pirozzoli et al. [25] confirms both the magnitude and the increase to within 0.03. A power law fitted to this surface therefore has one degree of freedom, not two: prefactor and exponent are tied by $\mathrm{d}\ln C/\mathrm{d}n = -\ln \mathrm{Re}_0$. The Dittus–Boelter pair (0.023, 0.8) is the tangent to the surface along the contour $n_{\text{eff}} = 0.8$, which passes through the classical calibration conditions; its prefactor is the structural compensation for its exponent, not an independent constant. The Bishop and Swenson pairs are displaced along the predicted locus with separations that recover their calibration Reynolds numbers, 1.7×10^5 and 4.9×10^5. Where C and n have been treated as independent fitted constants, they are coordinates of a single tangency.

The scope of both results is the smooth pipe with uniform properties, thermally fully developed, over $0.5 \leq \mathrm{Pr} \leq 16$. The weakest element of the closure is the core at low Prandtl number, where a substantial part of the resistance lies outside the log layer and is carried by the Reichardt factor and $\mathrm{Pr}_{t\infty}$ alone. There the $-7\,\%$ deviation from the isothermal-wall DNS resides. The thermal boundary condition contributes a further 2–4.5 % spread at $\mathrm{Pr} \approx 0.7$. Whether the drift of the exponent saturates above $\mathrm{Re}_\tau = 6000$ is open and requires simulation beyond the present databases.

The operational consequence follows from the rigidity. A power-law pair cannot follow a flow in which the local Reynolds and Prandtl numbers depart from the calibration window, and cannot be made to follow it by adjusting the exponent, since the prefactor is displaced with it. In constant-property flow the resulting detachment is a few per cent per decade of Reynolds number and constitutes the floor of the correlation error. Only a formulation that retains the logarithmic structure, in the manner of Petukhov and Kirillov and of Gnielinski, or that derives the Reynolds scaling anew for the regime concerned, removes it. Heat transfer at supercritical pressure, where the bulk Reynolds number varies severalfold and the bulk Prandtl number by an order of magnitude along one heated pipe, is the most demanding instance. The constant-property result established here is used, and tested against experimental data-base, in the companion study of that regime [17, 18].

Acknowledgments

This study was supported by TÜBİTAK, the Scientific and Technological Research Council of Türkiye, under Project No. 123M535, and by the European Union co-funded partnership CONNECT-NM under Grant Agreement No. 101165375.

Author declarations

Conflict of interest. The authors have no conflicts to disclose.

Data availability

The simulation Nusselt numbers used in Tables 1, 2 and 4 are those tabulated by Pirozzoli [23], Pirozzoli et al. [25] and openly available at http://newton.dma.uniroma1.it/database/. Those in Table 3 are from the dataset of Straub et al. [30] accompanying Straub et al. [29]. The correlation coefficients in Table 7 are those published in the sources cited.

References

[1] Guenter Ahlers, Siegfried Grossmann, and Detlef Lohse. Heat transfer and large scale dynamics in turbulent Rayleigh-Bénard convection. *Rev. Mod. Phys.*, 81:503–537, Apr 2009. doi:10.1103/RevModPhys.81.503.

[2] A.A. Bishop, R.O. Sandberg, and L.S. Tong. Forced convection heat transfer to water at near-critical temperature and supercritical pressures. Technical Report WCAP-2056, Westinghouse Electric Corporation, Pittsburg, USA, December 1964. (see also AICE, J. Chemical Engineering Symposium Series, No 2. London: Institute of Chemical Engineers, 1965).

[3] F. W. Dittus and L. M. K. Boelter. Heat transfer in automobile radiators of the tubular type. Technical Report 13, University of California, Berkeley, Calif., October 1930. Reprinted in International Communications in Heat and Mass Transfer, Vol. 12, pp. 3–22, 1985.

[4] J. G. M. Eggels, F. Unger, M. H. Weiss, J. Westerweel, R. J. Adrian, R. Friedrich, and F. T. M. Nieuwstadt. Fully developed turbulent pipe flow: a comparison between direct numerical simulation and experiment. *Journal of Fluid Mechanics*, 268:175–210, 1994. doi:10.1017/S002211209400131X.

[5] G.K. Filonenko. Hydraulic resistance in pipelines. *Teploenergetika (Therm. Eng.)*, 1(4):40–44, 1954. (in Russian).

[6] V. Gnielinski. Neue gleichungen für den wärme- und den stoffübergang in turbulent durchströmten rohren und kanälen. *Forschung im Ingenieurwesen A*, 41(1):8–16, 1975. ISSN 1434-0860. doi:10.1007/BF02559682.

[7] S. Grossmann and D. Lohse. Scaling in thermal convection: a unifying theory. *Journal of Fluid Mechanics*, 407:2756, 2000. doi:10.1017/S0022112099007545.

[8] J.D. Jackson. Fluid flow and convective heat transfer to fluids at supercritical pressure. *Nuclear Engineering and Design*, 264:24–40, 2013. ISSN 0029-5493. doi:10.1016/j.nucengdes.2012.09.040. SI:NURETH-14.

[9] B. A. Kader. Temperature and concentration profiles in fully turbulent boundary layers. *International Journal of Heat and Mass Transfer*, 24(9):1541–1544, 1981. doi:10.1016/0017-9310(81)90220-9.

[10] B. A. Kader and A. M. Yaglom. Heat and mass transfer laws for fully turbulent wall flows. *International Journal of Heat and Mass Transfer*, 15(12):2329–2351, 1972. doi:10.1016/0017-9310(72)90131-7.

[11] W. M. Kays and M. E. Crawford. *Convective Heat and Mass Transfer*. McGraw-Hill, New York, 3rd edition, 1993.

[12] Robert H. Kraichnan. Turbulent Thermal Convection at Arbitrary Prandtl Number. *Physics of Fluids*, 5(11):1374–1389, 11 1962. ISSN 0031-9171. doi:10.1063/1.1706533.

[13] R. N. Lyon. Liquid metal heat-transfer coefficients. *Chemical Engineering Progress Symposium Series*, 47(2):75–81, 1951.

[14] Ivan Marusic, Jason P. Monty, Marcus Hultmark, and Alexander J. Smits. On the logarithmic region in wall turbulence. *Journal of Fluid Mechanics*, 716:R3, 2013. doi:10.1017/jfm.2012.511.

[15] A. Moisseytsev and J. J. Sienicki. PDC: Plant Dynamics Code for Design and Transient Analysis of Supercritical Brayton Cycles. Technical Report ANL-ART-154, Nuclear Science and Engineering Division, Argonne National Laboratory, September 2018. URL https://publications.anl.gov/anlpubs/2018/10/146715.pdf. System-level code for steady-state and transient simulation of sCO_2 Brayton cycles; widely used for nuclear-coupled and other sCO_2 power systems.

[16] A. J. Musker. Explicit expression for the smooth wall velocity distribution in a turbulent boundary layer. *AIAA Journal*, 17(6):655–657, 1979. doi:10.2514/3.61193.

[17] I. Otić and Ö. Ertunç. The thermal impedance integral and the pathway decomposition of supercritical turbulent heat transfer. Part I. Framework. *KITopen preprint*, 2026. doi:10.5445/IR/1000196040.

[18] I. Otić and Ö. Ertunç. The thermal impedance integral and the pathway decomposition of supercritical turbulent heat transfer. Part II. Experimental validation and scope of the linearised pathway form. *KITopen preprint*, 2026. doi:10.5445/IR/1000196041.

[19] B. S. Petukhov and V. V. Kirillov. O teploperenose pri turbulentnom techenii zhidkosti v trubakh (about heat transfer in turbulent fluid flow in tubes). *Teploenergetika*, (4):63–68, 1958. In Russian.

[20] B.S. Petukhov. Heat transfer and friction in turbulent pipe flow with variable physical properties. In James P. Hartnett and Thomas F. Irvine, editors, *Advances in Heat Transfer*, volume 6 of *Advances in Heat Transfer*, pages 503–564. Elsevier, 1970. doi:10.1016/S0065-2717(08)70153-9.

[21] I.L. Pioro and R.B. Duffey. *Heat Transfer and Hydraulic Resistance at Supercritical Pressures in Power Engineering Applications*. ASME Press, New York, USA, 2007. doi:10.1115/1.802523. 334 p.

[22] S. Pirozzoli. Prandtl number effects on passive scalars in turbulent pipe flow. *Journal of Fluid Mechanics*, 965:A7, 2023. doi:10.1017/jfm.2023.387.

[23] S. Pirozzoli. An explicit representation for mean profiles and fluxes in forced passive scalar convection. *Journal of Fluid Mechanics*, 968:R1, 2023. doi:10.1017/jfm.2023.591.

[24] S. Pirozzoli, J. Romero, M. Fatica, R. Verzicco, and P. Orlandi. One-point statistics for turbulent pipe flow up to $Re_\tau \approx 6000$. *Journal of Fluid Mechanics*, 926:A28, 2021. doi:10.1017/jfm.2021.727.

[25] S. Pirozzoli, J. Romero, M. Fatica, R. Verzicco, and P. Orlandi. DNS of passive scalars in turbulent pipe flow. *Journal of Fluid Mechanics*, 940:A45, 2022. doi:10.1017/jfm.2022.265.

[26] H. Reichardt. Vollständige Darstellung der turbulenten Geschwindigkeitsverteilung in glatten Leitungen. *Zeitschrift für Angewandte Mathematik und Mechanik*, 31(7):208–219, 1951. doi:10.1002/zamm.19510310704.

[27] RELAP5. Webpage. https://inl.gov/relap53d/, 2026. last visited: 17.02.2026.

[28] Richard J. A. M. Stevens, Erwin P. van der Poel, Siegfried Grossmann, and Detlef Lohse. The unifying theory of scaling in thermal convection: the updated prefactors. *Journal of Fluid Mechanics*, 730:295308, 2013. doi:10.1017/jfm.2013.298.

[29] S. Straub, P. Forooghi, L. Marocco, T. Wetzel, R. Vinuesa, P. Schlatter, and B. Frohnapfel. The influence of thermal boundary conditions on turbulent forced convection pipe flow at two Prandtl numbers. *International Journal of Heat and Mass Transfer*, 144:118601, 2019. doi:10.1016/j.ijheatmasstransfer.2019.118601.

[30] S. Straub, P. Forooghi, L. Marocco, T. Wetzel, R. Vinuesa, P. Schlatter, and B. Frohnapfel. Statistics on turbulent forced convection pipe flow with different thermal boundary conditions for two Prandtl numbers. Dataset, Karlsruhe Institute of Technology, 2019.

[31] H.S. Swenson, J.R. Carver, and C.R. Kakarala. Heat transfer to supercritical water in smooth-bore tubes. *Trans. ASME, J. Heat Transfer, C*, 87(4):477–484, 1965. doi:10.1115/1.3689139.

[32] A Vasic, T Beuthe, H Zahlan, A Nava-Dominguez, and D Wang. State of the art report on heat transfer at supercritical pressures. *Canadian Nuclear Laboratories, Chalk River, ON, Canada*, 2023.